Far-infrared properties of resonant modes and tunnelling states in rare-earth-doped calcium fluoride

2001 J. Phys.: Condens. Matter 13 2095

(http://iopscience.iop.org/0953-8984/13/10/305)

INSTITUTE OF PHYSICS PUBLISHING JOURNAL OF PHYSICS: CONDENSED MATTER

J. Phys.: Condens. Matter **13** (2001) 2095–2116 www.iop.org/Journals/cm PII: S0953-8984(01)17319-4

Far-infrared properties of resonant modes and tunnelling states in rare-earth-doped calcium fluoride

S A FitzGerald[1], **A J Sievers**[2] **and J A Campbell**[3]

[1] Department of Physics, Oberlin College, Oberlin, OH 44074, USA
[2] Laboratory of Atomic and Solid State Physics and Cornell Center for Materials Science, Cornell University, Ithaca, NY 14853, USA
[3] Department of Physics, University of Canterbury, Christchurch, New Zealand

Received 20 September 2000

Abstract

The low-temperature observation of a broad distribution of two-level systems in chemically disordered fluorite mixed crystals has heightened interest in the spectroscopic properties of the corresponding lightly doped crystals. The low-temperature far-ir absorption of calcium fluoride crystals doped with Y^{3+}, La^{3+} or Lu^{3+} in the range less than 1 mol% shows three completely different types of defect-induced spectra and the temperature and concentration dependence are found to vary widely. In addition, the far-ir properties of CaF_2 doped with Y^{3+} or Lu^{3+} can be dramatically altered by heat treatment, indicating that clustering plays an important role. By comparing the spectroscopic signatures with those previously observed for other defect systems, the lowest-lying excitations for these doped CaF_2 crystals have been assigned as follows: tunnelling transitions in two different elastic configurations for Y^{3+}, a variety of ground state tunnelling transitions for the La^{3+} doping and an anharmonic resonant mode for the Lu^{3+} doped system. The surprising result is that a broad distribution of two-level systems is clearly evident in two of the three systems and the optical activity of this distribution appears to be controlled by the optical activity of the dominant defect dynamics.

1. Introduction

The near uniform distribution of low-lying two-level systems (TLS) in chemically disordered mixed crystals [1–7] and its similarity to the TLS distribution found in glasses [8–11] provides an opportunity to probe glass-like behaviour in a more ordered state and perhaps determine the minimum requirements for its development. An important experimental parameter in the mixed crystal work is the concentration of the dopant. High-concentration studies of mixed fluorites in the microwave [2] and in the far-ir [5] show that the TLS distribution is always observed and also that with increasing dopant concentration the TLS density of states appears to saturate at a level ($\sim 10^{18}$ cm^{-3}) comparable to that previously found in glasses [12]. Although there may be near universal TLS spectroscopic behaviour at high concentration, it is quite different from

the universality of the ac conduction of disordered solids observed at higher temperatures [13]. An important question is how do TLS evolve at low concentrations? The early work [14, 15] on the far-infrared properties of fluorite crystals doped with low concentrations of heavy trivalent impurities appeared to agree with defect theory [16]. However, the mm-wave frequency region was not explored in these initial studies and the later mm-wave measurements [17] were limited to the Y^{3+} doped CaF_2 system, studying the influence of hydrostatic pressure at low temperatures but not examining the temperature dependence of the spectrum. Given the variety of defect properties expected for anion-excess alkaline-earth fluorides [18, 19] it is perhaps not surprising that a systematic far-ir spectroscopic study on low-temperature samples is only now underway.

The study reported here has a somewhat narrow goal. It is to identify the evolution of TLS in fluorite crystals at low dopant concentrations. To do this the spectroscopic properties of three fluorite mixed-crystal systems ($(CaF_2)_{1-x}$:$(LaF_3)_x$, $(CaF_2)_{1-x}$:$(YF_3)_x$ and $(CaF_2)_{1-x}$:$(LuF_3)_x$) are examined in some depth for small x. An unusual find is that temperature and concentration dependent absorption spectra for all three systems are radically different even though at high concentrations each combination shows a distribution of both ground state and excited state TLS transitions [12]. The YF_3 doped samples possess a low-temperature spectrum which is dominated by a single sharp line at the lowest concentrations in agreement with the earlier study [17]. However the current temperature dependent study indicates that this sharp absorption band centred at 9.4 cm^{-1} is superimposed on a broad distribution of TLS. The LaF_3 doped samples possess a low-temperature far-ir spectrum which becomes increasingly complex and structured as the dopant concentration is decreased, i.e., at $x = 0.001$ there are more than six sharp ground state tunnelling transitions. The absorption spectra of LuF_3 doped samples is also dominated by a single sharp absorption line, centred at roughly 18 cm^{-1} at 1.4 K. This anharmonic lattice resonant mode shifts dramatically to higher frequency with increasing temperature. High-temperature thermal cycling is shown to reversibly alter the sharp line absorption spectra of $(CaF_2)_{1-x}$:$(YF_3)_x$ and $(CaF_2)_{1-x}$:$(LuF_3)_x$, while producing no effect in the spectra of LaF_3 doped samples.

The next section identifies key experimental details. Section 3 presents the experimental results. The spectra are subdivided by dopant type, with further subdivisions occurring by way of concentration dependence, sample heat treatment and temperature dependent spectroscopy. The discussion in section 4 identifies the different defect dynamics with the observed spectra. A careful examination of these three lattice-defect systems reveals evidence for yet another spectroscopic property, namely, a weak distribution of TLS in addition to the strong defect induced spectra. The conclusions follow.

2. Experimental details

Due to the small absorption coefficient for low dopant concentrations it is necessary to use quite long samples in order to achieve a measurable change in signal intensity. Generally the samples are ~5 cm in length; however, for some extremely weakly absorbing combinations lengths of up to 15 cm have been examined. In all cases the absorption coefficient of a lightly doped sample is determined by referencing its transmission spectrum to that of the pure crystal. The accuracy of the measurement is increased when temperature jump experiments are carried out since then the background radiation-induced change in the detector sensitivity is extremely small.

Single-crystal rods of doped fluorite crystals 1 cm in diameter and up to 5 cm long were grown at Canterbury using the Stockbarger technique. The starting material was held in a graphite crucible in vacuum, with PbF_2 as an oxygen getter. The crystal growth rates were

from a few mm to 12 mm per hour. The dopant concentration of the samples was checked using x-ray fluorescence.

Far-infrared transmission spectra were measured over the range 3 to 40 cm^{-1} using a lamellar grating interferometer in conjunction with a He^3 cooled bolometer detector. Up to five samples could be immersed in pumped liquid helium at 1.4 K and then later elevated in temperature using a small heater attached to the copper sample holder. The sample temperature was monitored with a carbon resistor thermometer throughout each scan. Low-temperature tests indicate that the temperature of the copper sample holder thermometer agrees with that of the sample to $\sim \pm 0.1$ K. For the higher frequency region (15–50 cm^{-1}) a Bomem DA3 Michelson interferometer was used together with a 1.6 K composite Si bolometer.

Samples for heat treatment were sealed in a quartz tube. Quenching was carried out by heating the sample to 900 °C for 18 hours and then quickly removing it to room temperature. Annealing was carried out by heating the sample to 625 °C for 18 hours, turning off the furnace and leaving it there until room temperature was reached.

3. Results

For the three defect systems of $(CaF_2)_{1-x}$:$(LaF_3)_x$, $(CaF_2)_{1-x}$:$(YF_3)_x$ and $(CaF_2)_{1-x}$:$(LuF_3)_x$ the data are presented in terms of both the temperature and concentration dependent absorption. The effects of high-temperature thermal cycling are also analysed for $(CaF_2)_{1-x}$:$(YF_3)_x$ and $(CaF_2)_{1-x}$:$(LuF_3)_x$. The $(CaF_2)_{1-x}$:$(LaF_3)_x$ system showed no effect with thermal cycling.

3.1. $(CaF_2)_{1-x}$:$(YF_3)_x$

3.1.1. Concentration dependence. Figure 1 presents the 1.4 K impurity-induced far-ir absorption spectra for a range of Y^{3+} concentrations. In figure 1(a) the absorption coefficient versus frequency is shown. The main feature is the broad line centred at 9.4 cm^{-1}, which disappears into a large defect induced background absorption at the highest concentration, $x = 0.04$. A second band at 4 cm^{-1} is also evident in the lower-concentration spectra. The properties of the central feature become clear in panel (b), where the absorption coefficient is divided by the dopant concentration. (Note that the sharp peak appears clipped due to the low resolution of the measurement.) For frequencies above the 9.4 cm^{-1} mode the concentration normalized background absorption increases with increasing concentration while the concentration normalized mode strength itself shows a complex dependence on concentration, first increasing but then decreasing. This normalized mode strength reaches a maximum in the region of $x = 0.001$ to 0.005 relative to the background.

The 1.4 K absorption spectra for the four lowest-concentration samples are shown in figure 2. The step in the impurity-induced absorption from one side of the transition to the other becomes more frequency independent with decreasing concentration. For $x = 0.0002$ the absorption changes from having a value for $\alpha < 0.002$ cm^{-1} at frequencies below 9.4 cm^{-1} to a constant value of $\alpha = 0.04$ cm^{-1} for frequencies above 9.4 cm^{-1}. The figure also shows the 9.4 cm^{-1} line width (FWHM) increasing from $\sim$1.2 cm^{-1} for $x = 0.0002$ to 1.9 cm^{-1} for $x = 0.001$. All four crystals have been annealed. This process enhances the relative strength of the 9.4 cm^{-1} band. Previously published results gave a width of 2.6 cm^{-1} for a similar YF_3 concentration [17]. A small frequency dependence of the absorption peak is observed. Although the height of the 9.4 cm^{-1} band is increased through annealing, its width is relatively unchanged. An as-grown $x = 0.0005$ sample has a width of 1.6 cm^{-1} in comparison to that of 1.4 cm^{-1} for the annealed sample.

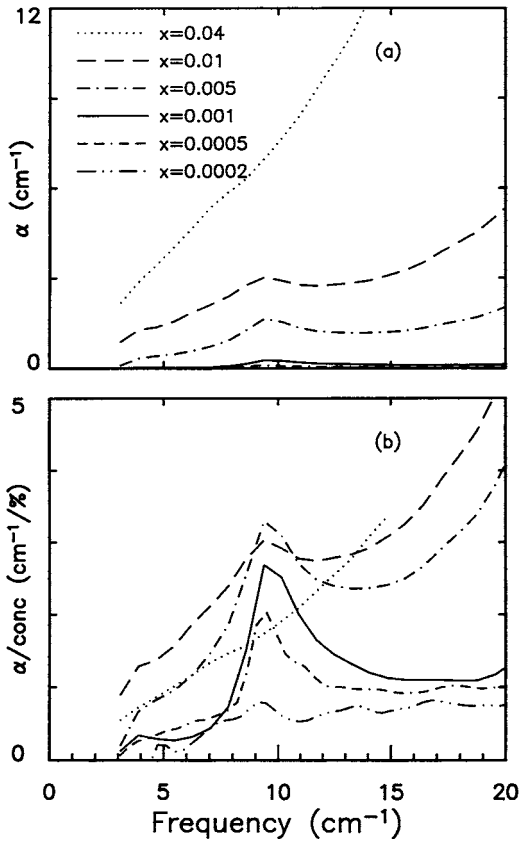

Figure 1. The 1.4 K absorption coefficient for the $(CaF_2)_{1-x}$:$(YF_3)_x$ system. (a) The absorption coefficient for the six lowest concentrations. The samples are all in their as-grown state. The resolution is 1.5 cm^{-1}. (b) The absorption coefficient normalized to the YF_3 concentration.

3.1.2. Heat treatment. Figure 3 presents the impurity-induced absorption coefficient versus frequency at two temperatures for the $x = 0.001$ sample after the sample had been heat treated in three different ways: as grown, annealed and quenched. Annealing the crystal strongly enhances the entire spectrum. At 1.4 K the solid curve shows that the background has been increased by a factor of two relative to that of an as-grown sample with the peak absorption at 9.4 cm^{-1} increasing by more than a factor of three. At 20 K the dashed curve indicates that the high-temperature band is enhanced by more than a factor of three as well. The absorption peak at 4 cm^{-1} is enhanced by a factor of ten through the annealing. In general the high-temperature band at 27.7 cm^{-1} and the low-temperature band at 9.4 cm^{-1} scale in the same way with heat treatment.

The quenching of a previously annealed sample reduces the background and the 9.4 cm^{-1} peak absorption by factors of roughly three and seven respectively as shown in figure 3. Despite the heat treatment induced changes in the absorption spectra shown here, the characteristic zero-crossing frequency (the frequency at which the absorption spectrum shows no temperature dependence) remains unchanged, independent of sample history. The effects of the heat treatment on the absorption spectrum are reversible, e.g. after repeated cycles of annealing followed by quenching the sample returns to its original annealed state without any noticeable change in the absorption spectrum. The percentage change in the absorption coefficient

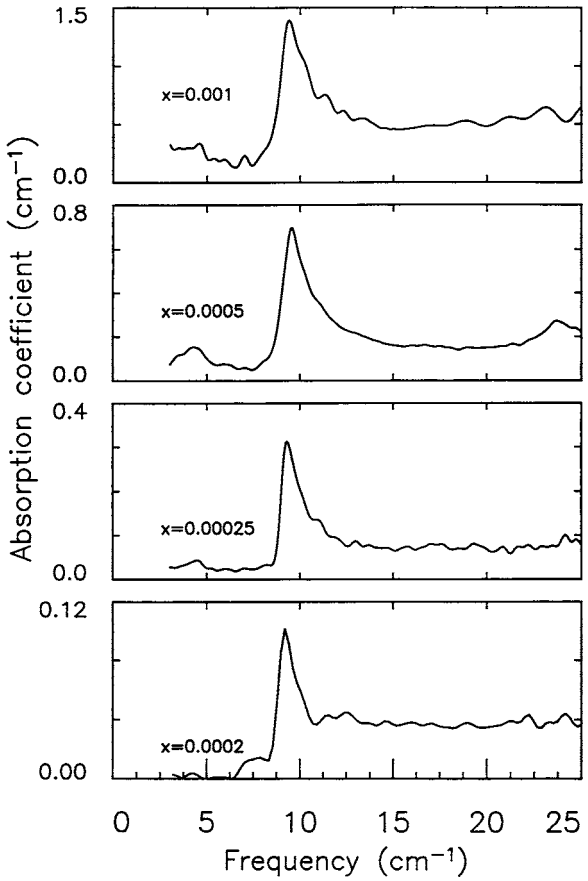

Figure 2. The concentration dependence of the 9.4 cm^{-1} band line shape for $(CaF_2)_{1-x}$:$(YF_3)_x$. All four samples have been annealed. The resolution is 0.4 cm^{-1}. Notice the absorption step between frequencies below the band and those above.

following annealing increases with decreasing dopant concentration. The $x = 0.0002$ sample shows a fivefold increase in the absorption strength of the 9.4 cm^{-1} band with an anneal relative to that of the as-grown sample.

During the heat treatment process in which the samples are at elevated temperatures in evacuated quartz tubes for many hours there is always the possibility that contaminants could be added to or withdrawn from the crystal. To test for these possibilities samples have been annealed in (1) quartz tubes under vacuum, (2) in quartz tubes under vacuum in the presence of an oxygen getter, PbF_2, and (3) simply standing in open air. In all three cases the heat treatment produced a similar effect on the sample's absorption spectrum. As a further test, three different samples were grown at three different rates. The first sample cooled from the melt temperature of 1423 °C at a rate of ∼300 °C h^{-1}; the second was cooled at ∼100 °C h^{-1}, and a third sample was cooled at ∼150 °C h^{-1}. The final rate of 150 °C h^{-1} is the standard used for normal samples. Qualitatively the spectra are consistent with the heat treatment results described above. The rapidly cooled sample shows a much weaker absorption than that of a slowly cooled sample, with the sample grown under normal conditions showing an intermediate absorption spectrum.

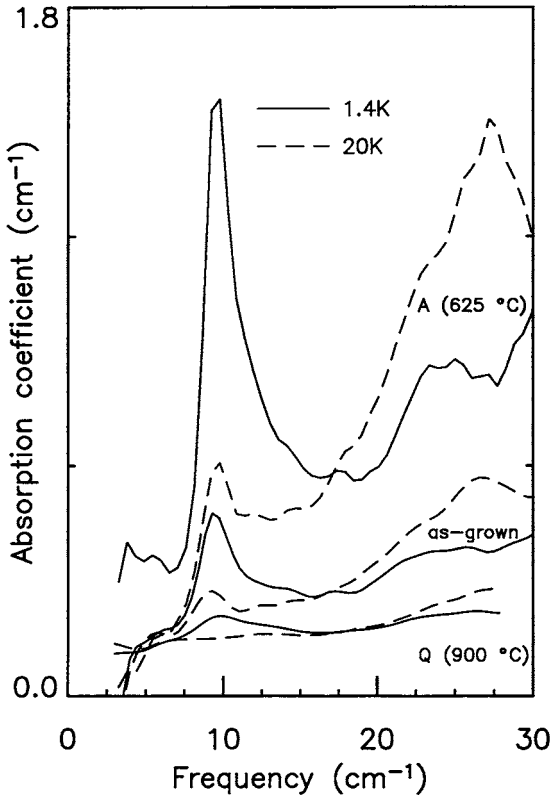

Figure 3. The effects of heat treatment on the absorption coefficient spectrum of $(CaF_2)_{0.999}$:$(YF_3)_{0.001}$. Two different temperatures are shown. (1) The as-grown state. (2) A = annealed. After heating under vacuum for 18 h at 625 °C and then cooling slowly to room temperature. (3) Q = quenched. After reheating to 900 °C for a further 18 h and then cooling rapidly to room temperature.

3.1.3. Temperature dependence. The temperature dependent absorption versus frequency of an annealed $(CaF_2)_{0.9995}$:$(YF_3)_{0.0005}$ sample is shown in figure 4 (top panel). Although these spectra are dominated by the 9.4 cm^{-1} band there remains weak temperature dependent absorption at other frequencies. The temperature-induced change in the absorption is plotted versus frequency in the lower panel of figure 4. To see if this temperature dependence obeys that expected for TLS the temperature-induced change in the absorption coefficient at the three frequencies shown in the figure (arrows) is plotted versus the thermal population difference, that is $\Delta P \equiv [\tanh(\hbar\omega/2kT_R) - \tanh(\hbar\omega/2kT)]$ according to equation (6) of [12].

These experimental results at the three frequencies of 5.5, 9.5 and 12.5 cm^{-1} are presented in figure 5. The lowest frequency of 5.5 cm^{-1} was chosen so as to minimize the contribution from both the 9.4 and 4.3 cm^{-1} bands. As pointed out in our earlier work [12] the temperature dependence of the TLS yields a straight line data set passing through the origin. For the frequencies above and below the absorption peak the temperature dependence shown in figure 5 follows the functional form predicted for the TLS. In contrast the data evaluated near the centre frequency of the 9.4 cm^{-1} band show a systematic deviation from TLS behaviour. This would indicate that for the low-concentration $(CaF_2)_{1-x}$:$(YF_3)_x$ system there exists a separate impurity band superimposed on top of a much weaker TLS spectrum.

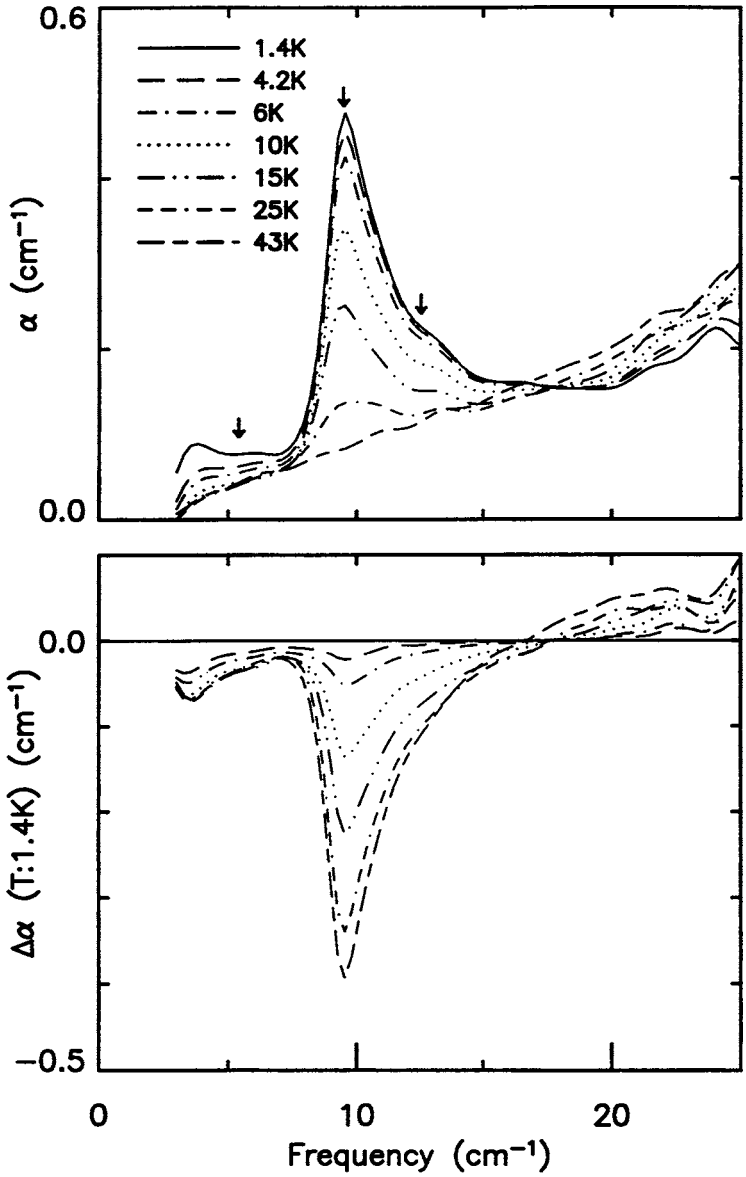

Figure 4. Temperature dependence of the absorption coefficient of $(CaF_2)_{0.9995}$:$(YF_3)_{0.0005}$ versus frequency viewed in two different ways. The sample was annealed. Top panel: The absorption coefficient for a range of temperatures from 1.4 to 43 K. With the exception of the 43 K curve there is a unique frequency ($\sim$16.6 cm^{-1}) at which the data show no temperature dependence. The three vertical arrows indicate the frequencies at which the temperature dependence of the data is analysed in the next figure. Lower panel: the temperature-induced change in absorption relative to that measured at 1.4 K. The resolution is 1.0 cm^{-1}.

The temperature dependence of a $(CaF_2)_{0.999}$:$(YF_3)_{0.001}$ sample over a larger spectral region (to 35 cm^{-1}) is displayed in figure 6. The strong temperature dependence of the 9.4 cm^{-1} mode is complemented by an equally strong inverse temperature dependence at a higher frequency. The temperature dependent line strengths can be examined with somewhat

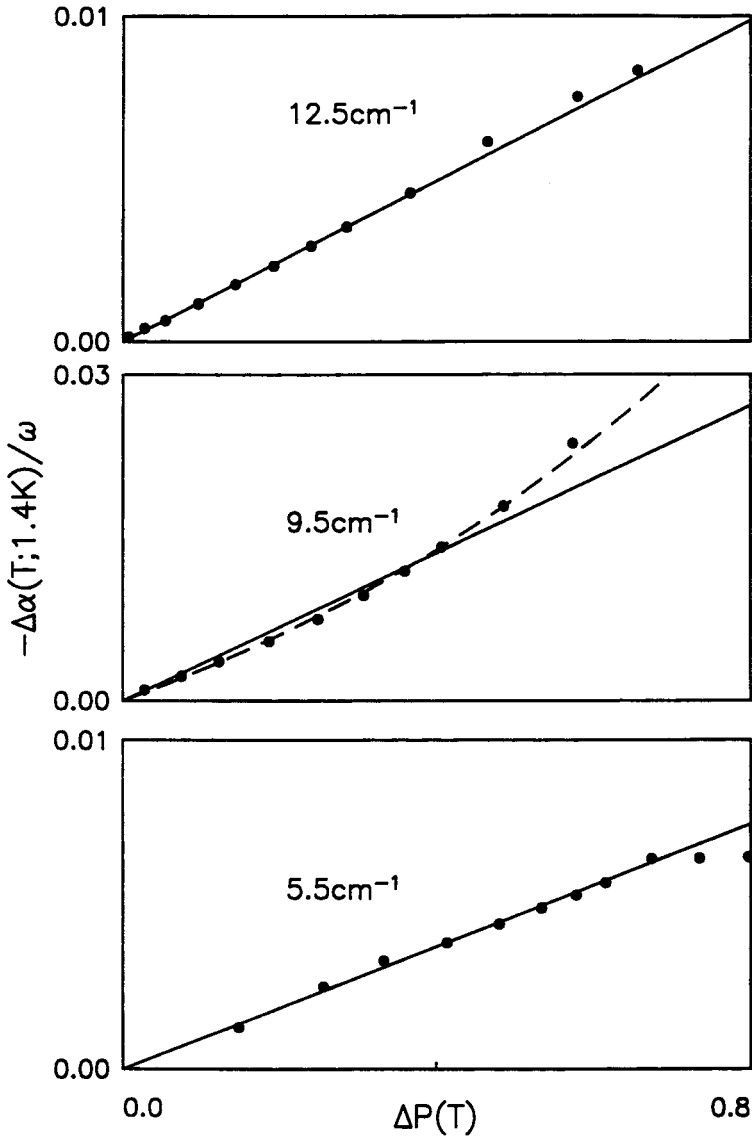

Figure 5. A comparison of theory and experiment for the temperature-induced change in the absorption coefficient of the $(CaF_2)_{0.9995}$:$(YF_3)_{0.0005}$ sample. The data are shown in figure 4. At 12.5 and 5.5 cm^{-1} the temperature dependence follows the linear form predicted by the TLS model. Near the mode frequency of 9.5 cm^{-1} the data deviate from the predicted linear TLS behaviour.

more precision by focusing on the temperature-induced change in absorption relative to that at 1.4 K shown in the lower panel. As the absorption decreases with increasing temperature for frequencies below $\sim$17 cm^{-1} it shows a corresponding increase in the 17 cm^{-1} to 35 cm^{-1} frequency region. Since all the curves from 1.4 to 25 K cross each other at 17.0 cm^{-1} there is one unique frequency at which the absorption coefficient shows no temperature dependence. This zero-crossing frequency for the temperature-induced change in absorption shifts by less than 10% over three orders of magnitude in concentration.

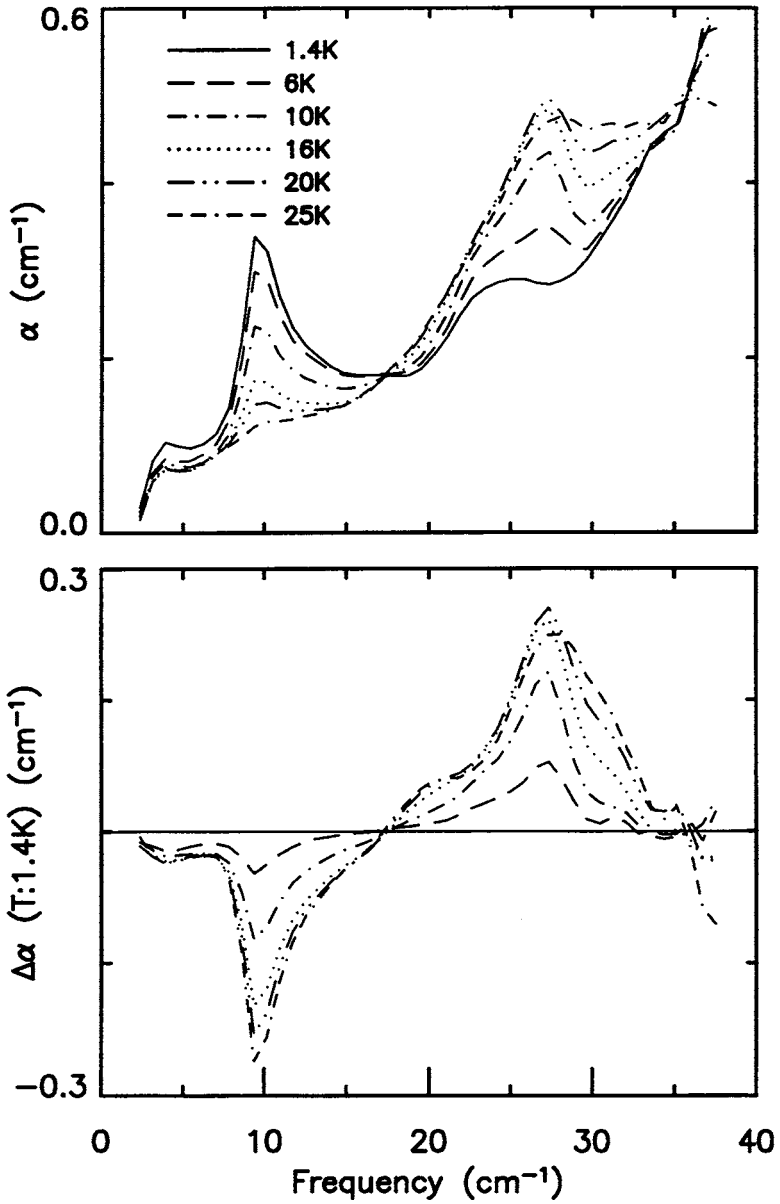

Figure 6. The temperature dependence of an as-grown $(CaF_2)_{0.999}$:$(YF_3)_{0.001}$ sample. Top panel: absorption coefficient for a range of temperatures from 1.4 to 25 K. Notice how the curves cross each other at the one frequency. Lower panel: the temperature-induced change in absorption relative to that at 1.4 K. Symmetry exists between the negative area centred at 9.4 cm^{-1} and the positive area at 27.7 cm^{-1}. The resolution is 1.5 cm^{-1}.

The 1.4 K absorption spectrum, shown in figure 6, contains two sharp bands, centred at 4 and 9.4 cm^{-1} respectively, and a broad feature at roughly 26 cm^{-1}. Measurements made with a Michelson interferometer indicate that the 26 cm^{-1} feature is comprised of two bands centred at 23 and 27.7 cm^{-1}. As the temperature is raised the intensity of the 27.7 cm^{-1} band increases reaching a maximum at $\sim$20 K. The strengths of all other absorption bands decrease

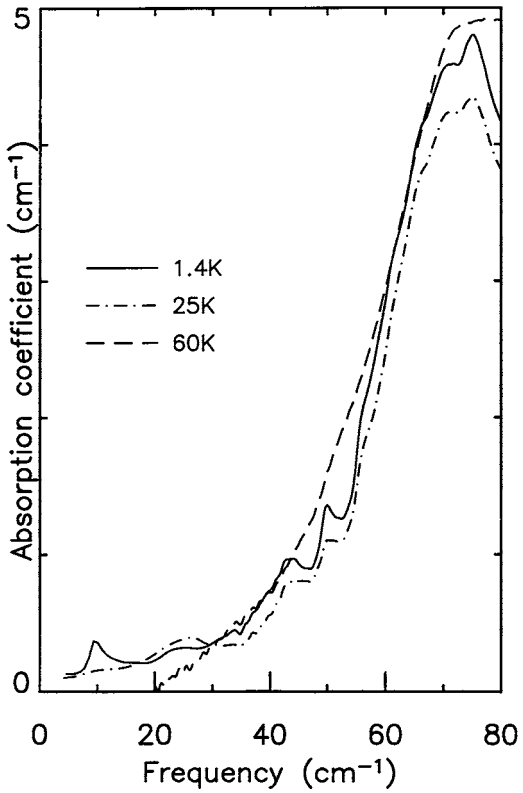

Figure 7. Temperature dependent absorption coefficient of $(CaF_2)_{0.999}$:$(YF_3)_{0.001}$ over a large frequency region. The resolution is 1.5 cm^{-1}.

monotonically with increasing temperature. The transfer of area with increasing temperature for the $\Delta\alpha$ curves in the lower panel indicates that the 9.4 and 27.7 cm^{-1} bands have a common origin, with the latter representing excited state transitions. These two bands also exhibit a similar concentration dependence.

Figure 7 shows the absorption coefficient versus frequency for $(CaF_2)_{0.999}$:$(YF_3)_{0.001}$ at 1.4 K over a still larger frequency interval, out to 80 cm^{-1}. Two additional sharp defect-induced features, centred at 43 and 50 cm^{-1} respectively, appear on the low-frequency side of a strong absorption band consisting of an unresolved doublet centred at about 72 cm^{-1}. A broad band centred at ∼80 cm^{-1} was previously attributed to a resonance mode resulting from the mass difference when the heavier Y^{3+} ion is substituted for Ca^{2+} [15].

3.2. $(CaF_2)_{1-x}$:$(LaF_3)_x$

3.2.1. Concentration dependence. The low-frequency 1.4 K absorption spectra for $(CaF_2)_{1-x}$:$(LaF_3)_x$ are shown for a range of concentrations in figure 8. High-temperature heat treatment produced no change in the spectra of these samples. The highest concentration, $x = 0.025$, shows a near featureless spectrum with a broad peak centred near 6 cm^{-1}. With decreasing concentrations sharper features emerge. The number of distinct bands increases from one at $x = 0.025$ to four at $x = 0.0025$ and there are possibly three additional bands for $x = 0.001$. For the lowest-concentration sample the four main bands are located at frequencies

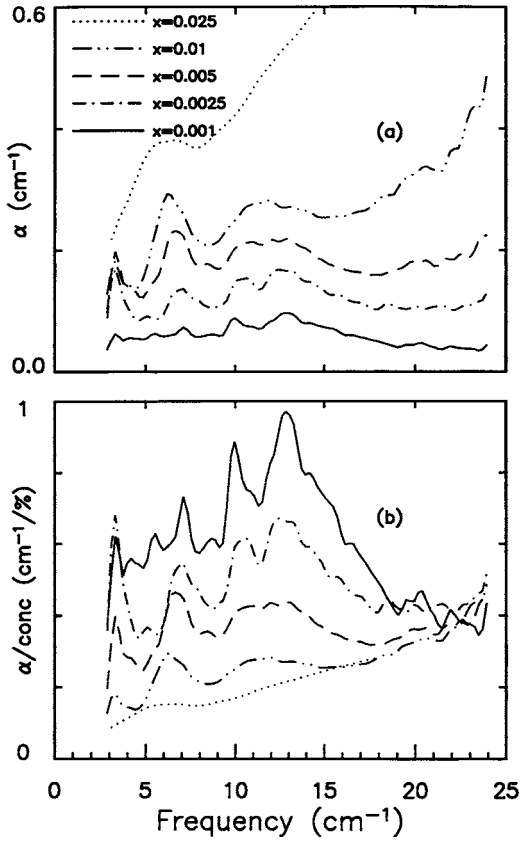

Figure 8. Low-temperature absorption coefficient versus frequency as a function of concentration for the $(CaF_2)_{1-x}$:$(LaF_3)_x$ system. (a) Absorption coefficient for the five lowest-dopant-concentration samples. The number of sharp features in a spectrum increases with decreasing concentration. (b) Absorption coefficient normalized by the concentration of LaF_3 in the sample. The induced absorption per dopant ion increases with decreasing concentration. The temperature is 1.4 K and the resolution is 0.5 cm^{-1}.

of 3.4, 7.1, 10.0 and 12.8 cm^{-1} respectively. The bands both broaden and shift in frequency with increasing concentration. The two higher-frequency bands shift towards each other while the 7.1 cm^{-1} band shows a large downward shift in frequency with increasing concentration, moving from 7.1 cm^{-1} at $x = 0.001$ to 6.2 cm^{-1} at $x = 0.01$. The 3.3 cm^{-1} band also appears to shift down in frequency with increasing concentration.

Figure 8(b) presents the absorption coefficient divided by dopant concentration versus frequency. Note that the absorption induced per impurity ion is largest for $x = 0.001$ and smallest for $x = 0.025$. A striking feature of these normalized absorption spectra is that they all cross at about the same frequency so that in the 21–23 cm^{-1} region the absorption per impurity ion appears constant. At this same frequency the higher-concentration $(CaF_2)_{1-x}$:$(LaF_3)_x$ samples, examined in [12], also showed no temperature dependence.

The impurity-induced absorption at 1.4 K is displayed in figure 9 for the three lowest-concentration samples extended out to 35 cm^{-1}. For all three samples the spectra in figure 9(a) are dominated by a higher-frequency doublet band. Higher-resolution data (resolution = 0.4 cm^{-1}) for the $x = 0.001$ sample reveals that the doublet peaks are centred

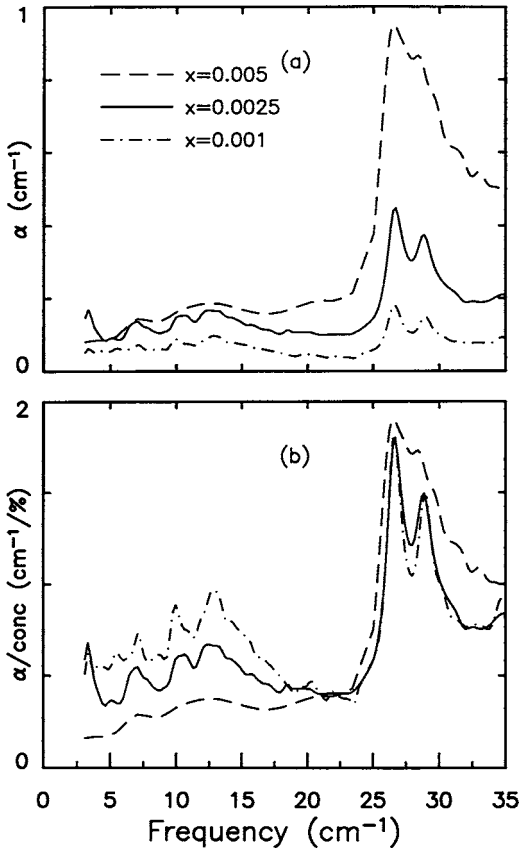

Figure 9. Absorption coefficient versus frequency for the $(CaF_2)_{1-x}$:$(LaF_3)_x$ system extended out to 35 cm^{-1}. (a) Absorption coefficient for the three lowest-concentration samples. The resolution is 0.5 cm^{-1} for frequencies below 20 cm^{-1} and 0.7 cm^{-1} for frequencies above. (b) The absorption coefficient normalized by the LaF_3 concentration. The relative strength of the high-frequency doublet increases while that of the modes below 20 cm^{-1} decreases.

at 26.5 and 28.7 cm^{-1} with FWHM of $\sim$0.8 cm^{-1}. These bands also broaden with increasing concentration. By $x = 0.005$ the doublet nature of the peak has almost disappeared. When the absorption coefficient is divided by the concentration, figure 9(b), an interesting trend becomes apparent. Although the features below 22 cm^{-1} decrease in the absorption per impurity ion, there is a comparable increase for features above that frequency. The low- and high-frequency parts of these spectra involve the same defect centre.

3.2.2. Temperature dependence. The solid lines in figure 10 represent the low-frequency absorption coefficient versus frequency for $(CaF_2)_{0.9975}$:$(LaF_3)_{0.0025}$ at a number of temperatures. (For practical reasons the resolution is now half of that displayed in figure 9.) The band strengths decrease with increasing temperature, without any apparent significant shift or broadening in frequency. The four main bands are clearly present at 9 K and their remnant remains even at 20 K.

Although these spectra are dominated by sharp features each entire spectrum bleaches with increasing temperature in a manner characteristic of tunnelling transitions. At these low frequencies, the temperature-induced change in absorption is negative, indicating that

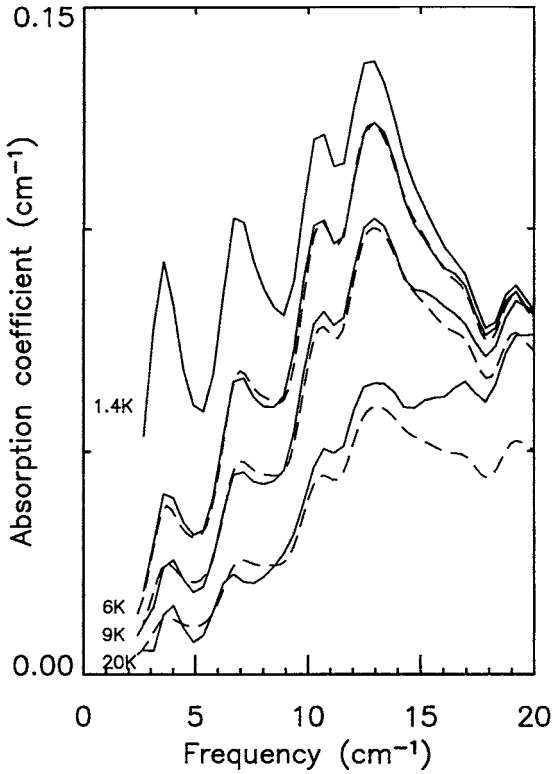

Figure 10. Temperature dependence of the $(CaF_2)_{0.9975}$:$(LaF_3)_{0.0025}$ absorption spectrum at low frequencies. The solid lines identify the measured absorption coefficient versus frequency at each temperature. The resolution is 1.0 cm^{-1}. The dashed lines show the theoretical absorption spectrum, at 6, 9 and 20 K, predicted for a distribution of TLS whose density of states has been determined from the experimental 1.4 K absorption curve. There are no free parameters with this approach.

it is dominated by a ground state absorption. To make a quantitative determination of the tunnelling component in figure 10, the 1.4 K spectrum is assumed to represent $G(\omega)$, the tunnelling optical density of states, which incorporates both the actual density and the dipole moment of the ir-active transitions [12]. This experimentally determined density of states at 1.4 K is then used to predict the absorption expected at all other temperatures. The dashed curves for 6, 9 and 20 K show the results for these predictions with no free parameters. The agreement with experiment is quite good. It is only at 20 K that we see a noticeable divergence between the model and the data at the higher frequencies. Note that a temperature independent contribution which has so far been ignored would contribute more at the higher-frequency end. For the low-concentration $(CaF_2)_{1-x}$:$(LaF_3)_x$ system and for temperatures below 15 K virtually the entire low-frequency ($\omega < 20$ cm^{-1}) absorption spectrum can be assigned to a number of ground state tunnelling transitions. Finally it should be noted that for temperatures up to 25 K all the absorption spectra cross each other at $\sim$22 cm^{-1}, the same frequency as observed in the high-concentration samples discussed in [12], and also the same frequency at which there is no concentration dependence to the normalized absorption displayed in figure 9.

The temperature dependent absorption coefficient for the higher-frequency doublet band for a $(CaF_2)_{0.999}$:$(LaF_3)_{0.001}$ sample is displayed in figure 11. Similar to the lower-frequency

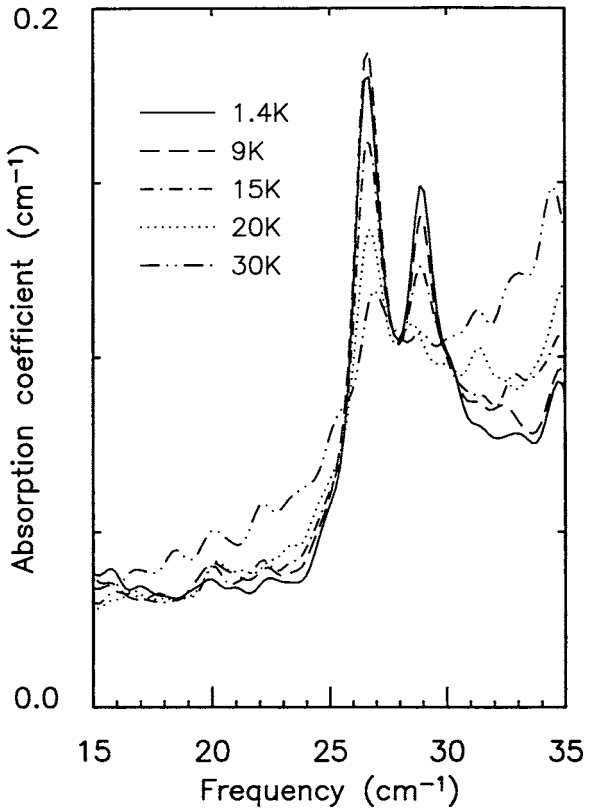

Figure 11. The temperature dependence of the $(CaF_2)_{0.999}$:$(LaF_3)_{0.001}$ doublet mode. The decrease in strength with increasing temperature indicates that these are ground state transitions. The resolution is 0.7 cm^{-1}.

bands shown in figure 10 these doublet features also become weaker at higher temperatures showing no broadening or shift in frequency with increasing temperature. The higher-frequency peak of the doublet band disappears quite dramatically for temperatures above 15 K. At 30 K there is no evidence for this band while its lower-frequency neighbour is still clearly present. The fact that the higher-frequency 28.7 cm^{-1} peak of the doublet band diminishes more quickly with temperature than the lower-frequency 26.5 cm^{-1} peak is a clear indication that each component in this doublet feature involves more than two levels. Although the lower-frequency peak of the doublet band appears to show an apparent increase in strength on warming from 1.4 to 9 K it is most likely caused by an increase in a much broader absorption band with increasing temperature. A similar dependence has been seen in higher-concentration samples. Figure 11 illustrates two effects with increasing temperature: a decrease in doublet line strength superimposed on an increasing broad background absorption. The small increase in area above 22 cm^{-1} is too small to represent the excited states of the low-frequency tunnelling states shown in figure 10.

The absorption spectrum at still higher frequencies contains two additional sharp bands centred at 48 and 61 cm^{-1}. Both bands are quite weak and decrease in strength with increasing temperature. Signal to noise limitations restricted data to below 90 cm^{-1}.

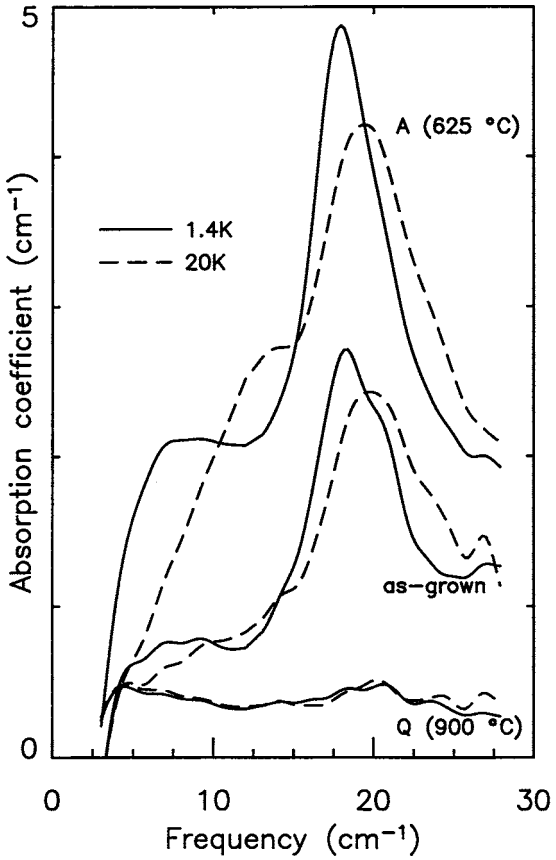

Figure 12. Influence of heat treatment on the absorption coefficient versus frequency for the $(CaF_2)_{0.998}$:$(LuF_3)_{0.002}$ sample. Two different temperatures are shown. (1) The as-grown state. (2) A = annealed. (3) Q = quenched. After reheating to 900 °C for a further 18 h and cooling rapidly to room temperature.

3.3. $(CaF_2)_{1-x}$:$(LuF_3)_x$

3.3.1. Heat treatment. The results of heat treatment on a low-concentration $(CaF_2)_{0.998}$:$(LuF_3)_{0.002}$ sample for two different temperatures are summarized in figure 12. The absorption coefficient for an as-grown sample is enhanced when it is annealed and greatly reduced when quenched. The quenched sample essentially shows no temperature dependence in its absorption coefficient, e.g. between 1.4 and 19 K the temperature-induced change in absorption is reduced by a factor of at least 25 relative to that of a annealed sample. The as-grown and annealed samples display similar frequency and temperature dependence in their spectra. In both cases the main band is centred at 18.4 cm^{-1} and shifts to higher frequency with increasing temperature.

The annealed sample exhibits a dramatic increase in the absorption below 10 cm^{-1}. Both the magnitude of the absorption and the temperature-induced change in absorption are increased by factors of three and five respectively. In contrast the strength of the 18 cm^{-1} band is only increased by a factor of two. The heat treatment results are quite similar to those shown in figure 3 for the $(CaF_2)_{1-x}$:$(YF_3)_x$ system, including the observation that the absorption at very low frequencies is strongly enhanced relative to the rest of the spectrum.

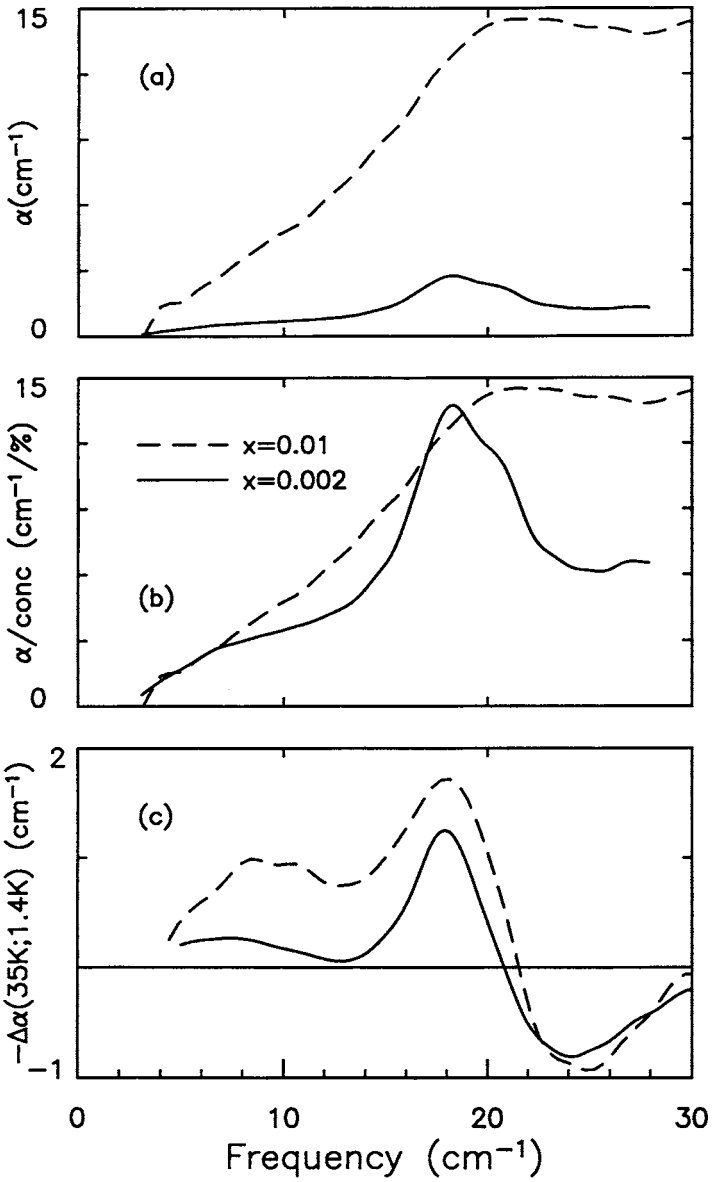

Figure 13. Low-temperature absorption properties versus frequency of CaF_2 doped with two different concentrations of LuF_3. Both samples are in their original as-grown state. The concentrations are given in the figure. (a) Absorption coefficient at 1.4 K. (b) Absorption coefficient normalized by the LuF_3 concentration. (c) Temperature-induced change in absorption coefficient between 1.4 and 35 K.

3.3.2. Concentration dependence. Figure 13(a) shows the 1.4 K absorption spectrum for $(CaF_2)_{1-x}$:$(LuF_3)_x$ with two different dopant concentrations. For $x = 0.002$ the absorption spectrum is dominated by a broad band which is centred at 18.4 cm^{-1}. The band has an FWHM of 6 cm^{-1}. For the higher-concentration $x = 0.01$ sample the band appears as a broad shoulder in the spectrum. Although it was only possible to examine two different concentrations

figure 13(b) demonstrates that generally the absorption strength is roughly proportional to the concentration. By examining both figures 13(a) and 13(b) it would appear that the 18.4 cm^{-1} band has either broadened or weakened dramatically on increasing the concentration from $x = 0.002$ to $x = 0.01$. However, figure 13(c), which shows the temperature-induced change in the absorption coefficient between 1.4 and 30 K, reveals that between the two concentrations there is almost no change in the strength of the temperature dependent peak at 18.4 cm^{-1}. Thus the strength of the temperature dependent 18.4 cm^{-1} band remains constant with increasing concentration, while the temperature independent background absorption increases roughly linearly with concentration. At the higher concentration the two effects superimpose in such a manner that the 18.4 cm^{-1} band appears as a small component on the temperature independent background absorption.

3.3.3. Temperature dependence. The temperature dependent absorption versus frequency for an as-grown $(CaF_2)_{0.998}$:$(LuF_3)_{0.002}$ sample is displayed in figure 14. The low-frequency range is presented in panel (a). At lower frequencies $\sim$7 cm^{-1} a broad absorption band is shown to decrease in strength with increasing temperature while at higher frequencies $\sim$12.5 cm^{-1} there is a corresponding increase in strength. (Also see the annealed sample case in figure 12.) The temperature-induced change in absorption is consistent with that of a broad distribution of TLS and is similar to that previously found at higher LuF_3 concentrations. The temperature dependent shift of the 18.4 cm^{-1} mode in the low-concentration samples limits the frequency range of study of TLS excited states.

The temperature dependent data over an expanded frequency region are shown in figure 14(b). The 1.4 K absorption spectrum is dominated by the band centred at 18.4 cm^{-1}. The strength of the Lu^{3+} induced band appears to be only weakly temperature dependent while the centre frequency of the band exhibits a very strong positive shift in frequency with increasing temperature. Between 1.4 and 50 K the band centre shifts from 18.4 to 23.3 cm^{-1}, with the total line strength decreasing by approximately 20%. At still higher temperatures the onset of a broad-band temperature activated absorption process distorts the shape of the resonant mode making it difficult to determine its exact width or centre frequency. There is one other weaker feature at 45 cm^{-1} which decreases in strength without any shift in frequency.

4. Discussion

The three related systems $(CaF_2)_{1-x}$:$(YF_3)_x$, $(CaF_2)_{1-x}$:$(LaF_3)_x$ and $(CaF_2)_{1-x}$:$(LuF_3)_x$ have produced three very different kinds of defect induced far-ir spectrum at low dopant concentrations indicating that a variety of defect dynamics processes are in play. To demonstrate that the strong impurity-induced spectral features can be described by defect processes which have been identified previously in simpler systems each defect system is now considered in turn.

4.1. Ground state tunnelling transitions in $(CaF_2)_{1-x}$:$(YF_3)_x$

The concentration dependent results shown in figure 1 indicate that the relative strength of the 9.4 cm^{-1} band reaches a maximum in the region of $x = 0.001$ to 0.005 and then decreases for higher concentrations. This concentration dependence eliminates any large complex clusters as the defect structures responsible for the 9.4 cm^{-1} band. Complex clusters become more not less abundant at higher concentrations. The pure alkaline-earth fluoride, MF_2 lattice consists of a cubic array of touching F^- ions with an M^{2+} ion in every second cell. Doping the pure material with RF_3 leads to the substitution of R^{3+} for M^{2+}, with charge neutrality being

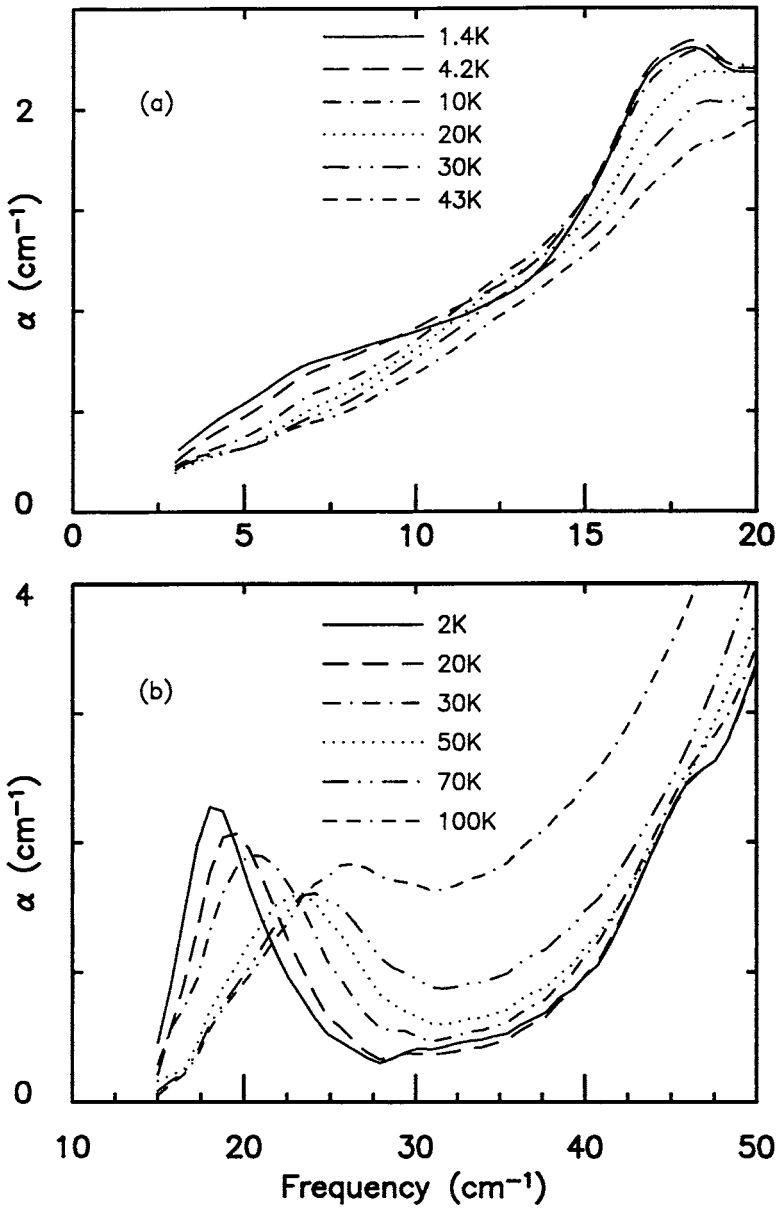

Figure 14. Temperature dependent absorption coefficient versus frequency of $(CaF_2)_{0.998}$:$(LuF_3)_{0.002}$. (a) Low-frequency data taken with the lamellar spectrometer. (b) High-frequency data taken with the Bomem DA3 Michelson spectrometer.

maintained by the addition of an F^- interstitial. At low dopant concentrations, $x < 0.001$, the large majority of the R^{3+} ions occur as single monomers, which are isolated from all other R^{3+} ions [20]. These defect structures consist of a single R^{3+} dopant ion with a compensating F^- interstitial. The F^- ion can sit in the NN position leading to a defect structure with tetragonal symmetry or it can sit in the NNN position in which case the symmetry is trigonal. It is also possible to have the compensating F^- interstitial several unit cells away from the R^{3+} ion in

which case defect site symmetry is cubic. The absolute number of these simple monomer structures reaches a maximum at dopant concentrations of $x \sim 0.01$, followed by a rapid decrease in numbers at higher concentrations, as more complex structures are formed [19]. For the $(CaF_2)_{1-x}$:$(YF_3)_x$ system the dominant monomer is that of the defect structure with tetragonal symmetry [21].

It is known that at low concentrations annealing a sample converts the simple tetragonal and trigonal monomer structures into complex clusters. Somewhat surprisingly this procedure also increases the number of simple monomers with cubic symmetry [22–24]. As the clusters, which are negatively charged, possessing more F^- interstitial ions than R^{3+} substitutional ions, form, they scavenge F^- interstitials from other defect structures, thereby converting previously tetragonal or trigonal site monomers into cubic sites. Our heat treatment results therefore preclude either tetragonal or trigonal monomers as possible sources for the 9.4 cm^{-1} band. A possible structure, consistent with both heat treatment and concentration results, is either a monomer off-centre in a cubic site or a simple dimer cluster.

If the 9.4 cm^{-1} band does arise from a ground state tunnelling transition then a possible explanation for the high frequency could be the presence of a strong internal electric field. For the KCl:Li tunnelling system the application of an external electric field dramatically increases the frequency of the observed tunnelling transition [25]. A field of 100 kV cm^{-1} leads to a transition frequency of the order of 10 cm^{-1}. Since a Y^{3+} ion with cubic symmetry will not experience a large internal electric field because the compensating F^- ion is, by definition, many unit cells away a more complex cluster must play a role. A simple electrostatics argument suggests that the defect charges could produce fields on the order of several hundred kV cm^{-1} at a tunnelling centre. The presence of such an asymmetry would both increases the energy splitting between levels, possibly as much as 10 cm^{-1}, while at the same time decreasing the strength of the allowed transitions.

4.2. Multiple elastic configurations

Numerical investigation shows that the large ratio of ground to excited state transitions for the $(CaF_2)_{1-x}$:$(YF_3)_x$ system precludes any model involving just a single anharmonic energy level scheme. The 9.4 and 27.7 cm^{-1} bands shown in figure 6 do appear to be intimately connected. The temperature-induced decrease in absorption strength of the 9.4 cm^{-1} line is mirrored by a roughly equal increase in the strength of the 27.7 cm^{-1} line. All the absorption curves for temperatures between 1.4 and 25 K cross each other at the same frequency of 17.0 cm^{-1}. The only band for which it is possible to obtain a precise temperature dependence, namely that at 9.4 cm^{-1}, exhibits a behaviour which is systematically different from the predictions of any simple two- or three-level model. The dashed curve shown in the centre panel of figure 5 actually corresponds to the dependence predicted for four equally spaced levels rather than two.

It appears that the absorption bands shown in figure 6 may arise from more than one elastic configuration with the ground state tunnelling transitions involving one configuration while the 'excited state' transitions appear in another. Such temperature dependent spectroscopic complexity has already been identified for the simple point defect system KI:Ag^+. Even at low temperatures two elastic configurations have been identified, which are separated by a large energy barrier but involve the same Ag^+ impurity [26]. Each elastic configuration is found to have its own defect-induced far-ir spectrum and as temperature is increased from 1.4 K the spectroscopic area is transferred from one to the other.

4.3. Ground state tunnelling transitions in $(CaF_2)_{1-x}$:$(LaF_3)_x$

The fact that such a complex tunnelling spectrum exists for $(CaF_2)_{1-x}$:$(LaF_3)_x$ provides a different perspective on the possible defect dynamics. Figure 9 shows that with increasing concentration the relative strength of the low-frequency tunnelling transitions decrease with respect to the higher-frequency modes in the 27 cm^{-1} frequency region. However, the temperature dependence measurements in figures 10 and 11 clearly demonstrate that all of these excitations are ground state transitions. One explanation, consistent with the data, is that the increased impurity concentration is producing stress- and electric field-induced dichroism in the admittedly complex, low-concentration tunnelling spectrum. Such effects have been reported for the Ag^+ tunnelling centre in RbCl [27]. Controlled stress and electric-field studies on low-temperature samples show how the oscillator strength of a tunnelling centre can be transferred from one far-ir frequency region to another even though the high-frequency transition frequencies remain essentially unchanged.

A most important observation is that no evidence of excited state transitions appears in figure 11 for temperatures up to 20 K; the spectrum is dominated by ground state transitions. Hence the low-frequency tunnelling features shown in figure 10, which disappear over that same temperature range, cannot be the same ones as are observed at large La^{3+} concentrations in [12] since in that case the corresponding excited state transitions are readily seen since their oscillator strengths are comparable to the ground state transitions.

4.4. Anharmonic resonant mode in $(CaF_2)_{1-x}$:$(LuF_3)_x$

An entirely different feature of the $(CaF_2)_{1-x}$:(LuF_3) system, shown in figure 14(b), is the defect-induced resonant mode. Even though the ionic sizes of Lu^{3+} and Y^{3+} are essentially the same, and both defect systems show a dramatic heat treatment annealing effect, the temperature dependence is completely different from that of $(CaF_2)_{1-x}$:(YF_3). With increasing temperature the Lu^{3+} resonant mode exhibits a large positive shift to higher frequencies. Two other standard defect systems which possess a low-frequency resonant mode, CsI:Tl^+ [28] and CsBr:Tl^+ [29], show such an anharmonic shift, although the magnitude is somewhat smaller. The CsBr:Tl^+ system has been measured reliably over the temperature interval from 1.4 to 77 K resulting in a shift of $\sim$2 cm^{-1}, from 16.5 to 18.5 cm^{-1}. For comparison the $(CaF_2)_{1-x}$:$(LuF_3)_x$ resonant mode shows a shift of $\sim$5.5 cm^{-1}, from 18.5 to 24 cm^{-1}, over the same temperature interval.

But most significant is the weak TLS spectrum which is evident in figure 14(a) at frequencies below the resonant mode. As the temperature increases and the resonant mode moves to higher frequencies the low-frequency TLS excited state band also becomes evident. This signature is quite reminiscent of that previously found for the high-concentration ($x = 0.1$) system [12].

4.5. Two-level systems

In the mm-wave region a distribution of TLS has been identified for all three systems but the actual evolution of TLS in fluorite crystals is clouded by the fact that the prominent spectral features are so different. One straightforward approach to describe the TLS in high-concentration fluorite mixed crystals is to assume that there would be sharp tunnelling transitions at very low concentration but that random strains build up as the defect density increases producing an ever widening spectrum of potential minima between which ions can tunnel [30, 31]. The concentration dependences of the spectra for $(CaF_2)_{1-x}$:$(YF_3)_x$ shown in figure 1, for $(CaF_2)_{1-x}$:$(LaF_3)_x$ in figure 8 and for $(CaF_2)_{1-x}$:$(LuF_3)_x$ in figure 13 clearly show such behaviour for strong defect modes whether or not tunnelling exists. This is often referred

to as inhomogeneous broadening. However, at low concentration the tunnelling transitions are not always sharp. Compare the broad TLS spectral features identified at two of the three arrows in figure 4 for the 0.0005 mol% Y^{3+} doping with the TLS for many sharp transitions in figure 10 for the 0.0025 mol% La^{3+} and also with the broad TLS below 10 cm^{-1} in figure 14(a) for the 0.002 mol% Lu^{3+} sample. The fact that the tunnelling level spectrum appears broad at low dopant concentration for two out of the three systems indicates that there is probably a distribution of such tunnelling levels already at these low impurity concentrations. It now seems likely that such a TLS distribution may occur for all three combinations but simply be hidden, or partially hidden, under a strong defect spectrum.

5. Conclusions

For dopant concentrations below $x = 0.01$ the far-ir spectra of the $(CaF_2)_{1-x}$:(RF_3) systems, where R = Y^{3+}, La^{3+} or Lu^{3+}, have been studied in some detail. Spectroscopic data were obtained as a function of dopant concentration, heat treatment and temperature dependence. The results below 40 cm^{-1} demonstrate that the dominant dynamical feature of each system produces a distinct and recognizable impurity-induced spectrum. For Y^{3+} doping both ground state and excited state tunnelling transitions appear, for La^{3+} only ground state tunnelling transitions are evident while for Lu^{3+} a temperature dependent resonant mode is the main feature. These features can be compared successfully, albeit in a qualitative manner, with those previously found in other defect–lattice systems.

In this work it is found that a careful examination of these three lattice-defect systems reveals evidence for yet another spectroscopic property, namely, a weak distribution of TLS in addition to the strong defect induced spectra. This featureless distribution is somewhat hidden by the dominant temperature dependent properties of the tunnelling spectrum for Y^{3+} and can only be observed on each side of the main transition at 9.4 cm^{-1}. For the case of La^{3+} where many low frequency tunnelling transitions are evident the absence of corresponding excited state transitions, which is a hallmark property of TLS for higher concentration mixed crystals and also for glasses, demonstrates that these tunnelling transitions cannot be identified with the TLS. The only system where both the TLS transitions and the TLS excited state transitions can be clearly identified at low concentration is for Lu^{3+} doping where the resonant mode defect induced spectrum appears at much higher frequencies than the entire TLS spectrum.

A consistent picture emerges if one assumes that the TLS spectrum actually occurs for all three systems but that its optical activity is controlled by the optical activity of the dominant defect dynamical component. Because the strongest features for the La^{3+} system show a greatly reduced optical activity when compared to the other two defect systems it is only here that evidence for the broad TLS distribution cannot be measured optically for these low concentrations.

Acknowledgments

We have benefited from discussions with R H Silsbee. This work is supported by NSF-DMR-9979483, NASA-MAG5-9140 and NASA-NAG8-1666.

References

[1] Walker F J and Anderson A C 1984 *Phys. Rev.* B **29** 5881
[2] Kazanskii S K 1985 *JETP Lett.* **41** 224
[3] Cahill D G and Pohl R O 1989 *Phys. Rev.* B **39** 10 477

[4] Love S P, Mungan C E, Sievers A J and Campbell J A 1992 *J. Opt. Soc. Am.* B **9** 794
[5] FitzGerald S A, Campbell J A and Sievers A J 1994 *Phys. Rev. Lett.* **73** 3105
[6] Tu J J, Campbell J A and Sievers A J 1997 *Mater. Sci. Forum* **239–241** 485
[7] Tu J J and Sievers A J 1999 *Phys. Rev. Lett.* **83** 4077
[8] Phillips W A 1981 *Amorphous Solids* ed W A Phillips (Berlin: Springer)
[9] Hunklinger S and Raychaudhuri A K 1986 *Progress in Low Temperature Physics* ed D F Brewer (Amsterdam: North-Holland) p 265
[10] Phillips W A 1987 *Rep. Prog. Phys.* **50** 1657
[11] Berret J F and Meißner M 1988 *Z. Phys.* B **70** 65
[12] FitzGerald S A, Sievers A J and Campbell J A 2001 *J. Phys.: Condens. Matter* **13**
[13] Dyre J C and Schrøder T B 2000 *Rev. Mod. Phys.* **72** 873
[14] Hayes W, Wiltshire M C, Manthey W J and McClure D S 1973 *J. Phys. C: Solid State Phys.* **6** L273
[15] Hayes W, Wiltshire M C K, Berman R and Hudson P R W 1973 *J. Phys. C: Solid State Phys.* **6** 1157
[16] Catlow C R A, Hayes W and Wiltshire M C K 1977 *J. Phys. C: Solid State Phys.* **10** L243
[17] Campbell J A, Schiff E A and Sievers A J 1975 *Phys. Lett.* A **51** 470
[18] Catlow C R A 1976 *J. Phys. C: Solid State Phys.* **9** 1845
[19] den Hartog H W 1994 *Defects and Disorder in Crystalline and Amorphous Solids* ed C R A Catlow (London: Royal Institute of Great Britain) p 435
[20] Hull S and Wilson A C 1992 *J. Solid State Chem.* **100** 101
[21] Cirillo-Penn K M and Wright J C 1990 *Phys. Rev.* B **41** 10 799
[22] Yanney P P, Schaeffer D M and Wolf J L 1975 *Phys. Rev.* B **11** 2460
[23] Franklin A D 1976 *J. Chem. Phys.* **64** 1509
[24] Tallant D R, Moore D S and Wright J C 1977 *J. Chem. Phys.* **67** 2897
[25] Kirby R D, Hughes A E and Sievers A J 1970 *Phys. Rev.* B **2** 481
[26] Sievers A J and Lai R 1998 *Physica* D **119** 205
[27] Barker A S and Sievers A J 1975 *Rev. Mod. Phys.* **47** S1
[28] Genzel L, Prettl W and Siep E 1969 *Optics Commun.* **1** 28
[29] Prettl W and Siep E 1971 *Phys. Status Solidi* b **44** 759
[30] Watson S K 1995 *Phys. Rev. Lett.* **75** 1965
[31] Liu X, Vu P D, Pohl R O, Schiettekatte F and Rooda S 1998 *Phys. Rev. Lett.* **81** 3171